

Elusive hot stripped helium stars in the Galaxy

I. Evolutionary stellar models in the gap between subdwarfs and Wolf-Rayet stars

L. Yungelson^{1,2}, A. Kuranov³, K. Postnov³, M. Kuranova⁴, L. M. Oskinova¹, and W.-R. Hamann¹

¹ Institut für Physik und Astronomie, Universität Potsdam, Karl-Liebknecht-Str. 24/25, 14476 Potsdam, Germany
e-mail: yungelson@astro.physik.uni-potsdam.de

² Institute of Astronomy, Russian Academy of Sciences, 48 Pyatnitskaya Str., Moscow 119017, Russia

³ Sternberg Astronomical Institute, M.V. Lomonosov Moscow State University, 14 Universitetsky Pr., Moscow 119992, Russia

⁴ Faculty of Computational Mathematics and Cybernetics, M.V. Lomonosov Moscow State University, 1-52 Leninskiye Gory, Moscow 119991, Russia

Received 25 August 2023 / Accepted 29 November 2023

ABSTRACT

Context. Stellar evolution theory predicts the existence of helium-core remnants of the primary components of intermediate-mass close binaries that lost most of their hydrogen-helium envelopes due to the mass exchange. These remnants are expected to be observed as hot helium-rich stars with masses of $(1-7) M_{\odot}$, located in the area of the Hertzsprung-Russell diagram between OB subdwarfs and Wolf-Rayet stars. While several thousands of such stripped helium stars are expected to exist in the Galaxy, none of them have been identified so far.

Aims. We aim to provide comprehensive predictions of the numbers and fundamental properties of stripped helium stars and their binary companions in the Galaxy. This is a necessary first step to guide observations, to enable a comparison between binary evolution models and realistic stellar populations, and to determine the feedback parameters of stripped helium stars in the Galaxy.

Methods. We expanded the previously considered space of parameters describing close binary systems producing stripped helium stars and applied a population synthesis based on a grid of evolutionary models computed by the code MESA, using a spin-dependent algorithm for the treatment of mass and angular momentum loss from the system.

Results. We show that the number of Galactic binaries hosting $(1-7) M_{\odot}$ He-stars is $\approx 20\,000$ and that it steeply declines with an increase in the He-star mass (≈ 3000 with mass $\gtrsim 2 M_{\odot}$). The decisive factor that defines the low number of stripped He-stars is runaway mass-loss after Roche lobe overflow (RLOF) by primary components of the binaries, which leads to the formation of common envelopes and the further merger of components. This effect strongly restricts the initial ranges of masses of components of the progenitors of stripped stars and orbital periods. In addition, stripped helium stars are much less numerous than expected, since a significant fraction of binaries in which the primaries have masses less than $(5-7) M_{\odot}$ produce subdwarfs with masses $\lesssim 1 M_{\odot}$. Our calculations show that the overwhelming majority of helium stars reside in binaries with an early-type companion star and can be identified neither by the UV excess nor by emission features. The large periods of a significant fraction of binaries hosting stripped stars (\gtrsim several hundred days) also hamper their discovery.

Key words. methods: numerical – stars: evolution – stars: mass-loss

1. Introduction

Mass exchange between components in close binary systems may occur at different evolutionary phases. In the so-called “case A”, mass exchange happens if the primary component overflows its Roche lobe (RLOF) in the main sequence. “Case B” mass exchange occurs if RLOF happens when the hydrogen shell burning is the main energy source of the star, before helium is ignited in the core. After pioneering works by Kippenhahn & Weigert (1967), Kippenhahn et al. (1967), Paczyński (1967), Kippenhahn (1969), Refsdal & Weigert (1969), Barbaro et al. (1969), Giannone et al. (1970), Lauterborn (1970), Ziolkowski (1970), Harmanec (1970), Giannone & Giannuzzi (1972), De Loore et al. (1974) it is accepted that at the solar metallicity ($Z = Z_{\odot}$), case B mass transfer results in the formation of a system with a He white dwarf (WD) component, if the zero-age main sequence (ZAMS) donor mass is $\lesssim 2.5 M_{\odot}$, or a hot ($\log(T_{\text{eff}}) \gtrsim 4.4$) stripped helium star (HeS star) component, if the donor’s ZAMS mass is higher

and the mass-loss by its stellar wind does not prevent RLOF. As we show below, HeS stars may also result from case A mass exchange if fast rotation of the close binary components is taken into account.

Stripped helium stars are nondegenerate He-cores of stars that retained a $\lesssim 1 M_{\odot}$ hydrogen-helium envelope, with the chemical abundance profile formed by several processes: the retreat of an H-burning convective core in the main sequence stage, mixing, further mass-loss during RLOF, and stellar wind from the post-RLOF remnant.

A special interest in the HeS stars stems from the fact that they are likely among the progenitors of both hydrogen-poor and hydrogen-rich core-collapse supernovae (SNe) if the mass of their CO core after He-exhaustion exceeds $\approx 1.4 M_{\odot}$ (Habets 1986), see also Uomoto (1986), Nomoto et al. (1994), Podsiadlowski (1996), Waldman et al. (2008), Kim et al. (2015), Yoon et al. (2017), Dessart et al. (2020), as well as progenitors of the electron-capture SNe and SNe Ia (Chanlaridis et al. 2022).

Furthermore, since HeS stars are hot and young, they might be copious sources of ionizing photons in star-forming galaxies (Dionne & Robert 2006; Götberg et al. 2018; Doughty & Finlator 2021).

In the Galaxy, $M \lesssim 2 M_{\odot}$ stars with hydrogen-depleted envelopes are usually identified as sdO/B-type subdwarfs (Iben & Tutukov 1985, 1987; Tutukov & Iungelson 1987; Howarth & Heber 1990; Tutukov & Yungelson 1990), while stripped stars with $M \gtrsim 7 M_{\odot}$ are identified with Wolf-Rayet (WR) stars¹ (Paczyński 1967). The mass gap between $2 M_{\odot}$ and $7 M_{\odot}$ is thought to be filled by HeS stars.

In the Galaxy, about 6000 sdO/B subdwarfs are detected within $\lesssim 5$ kpc of the Sun (Geier 2020). The estimates of the total number of WR stars in the Galaxy range from 1200 ± 100 (Crowther 2015) to about 2600 (Kanarek 2017), with 669 objects having already been identified². However, currently only a dozen sdO-stars with estimated periods and mass $\gtrsim 1 M_{\odot}$ have been found in binaries (see Table 9 in Wang et al. 2023). All of them are companions of Be-stars³. Yet, HR 6819 (Bodensteiner et al. 2020) and NGC 1850 BH1 (El-Badry & Burdge 2022), with estimated subdwarf masses $\sim 1 M_{\odot}$ may belong to the same type of stars. There are also several semidetached systems with masses of donors about $(0.8\text{--}0.9) M_{\odot}$, which may be expected to be progenitors of massive subdwarfs, “cousins” of HeS stars, for example DQ Vel (Barría et al. 2013), V495 Cen (Rosales Guzmán et al. 2018), HD 15124 (El-Badry et al. 2022), and V1315 Cas (Zak et al. 2023). Interestingly, only one “canonical” subdwarf companion ($M = 0.426 \pm 0.043 M_{\odot}$) to a Be-star ($M = 3.65 \pm 0.48 M_{\odot}$) has been directly observed (κ Dra, Klement et al. 2022).

Shenar et al. (2020a) disentangled the spectrum of the Galactic star LB-1 (Liu et al. 2019) and suggested that it harbors a $1.5 \pm 0.4 M_{\odot}$ stripped star with a $(7 \pm 2) M_{\odot}$ Be companion. However, Hennicker et al. (2022) have shown that the modeling of the H α profile in the spectrum of this binary still does not rule out an alternative hypothesis, according to which LB-1 could host a B-star and a black hole.

The Galactic star γ Columbae is nitrogen-enriched and has $T_{\text{eff}} = 15\,500 \pm 340$ K. Given its estimated $\log(g) = 3.3 \pm 0.01$, the spectroscopically determined mass is $\sim 4 M_{\odot}$ (Irrgang et al. 2022). This led Irrgang et al. (2022) to suggest that γ Col is a remnant of an initially $12 M_{\odot}$ component of a binary that was stripped in a common envelope event and that is currently readjusting its structure to become a hot, compact object. However, no traces of a companion have been found so far, which raises questions about this interpretation.

The helium star in the HD 45166 system, the famous qWR object, was considered as a prototype of a $4 M_{\odot}$ HeS star and

used to anchor the theoretical prescription of the mass-loss rate in the evolutionary models. Recently, it was recognized that the qWR star in HD 45166 is most likely a strongly magnetic merger product ($M = (2.03 \pm 0.44) M_{\odot}$) and that its wind is highly affected by the presence of the magnetic field (Shenar et al. 2023).

Thus, no HeS star with $M \approx (2\text{--}7) M_{\odot}$ has unequivocally been detected in the Galaxy.

In nearby low-metallicity galaxies, the number of suspected HeS stars is growing. Recently, Ramachandran et al. (2023) discovered that a double-line spectroscopic binary, SMCSGS-FS 69, in the Small Magellanic Cloud (SMC, $Z \approx 0.2 Z_{\odot}$) harbors an object resembling a HeS star. The object is quite massive, with $M_{\text{HeS}} = 2.8^{+1.5}_{-0.8} M_{\odot}$. Its companion is a $M_{\text{Be}} = 17^{+9}_{-7} M_{\odot}$ Be-star. Ramachandran et al. (2023) found a strongly enhanced N-abundance and moderately enhanced He-abundance in the envelope of a HeS star in the SMCSGS-FS 69, suggesting that the stripping was only partial and that the primary retained a significant fraction of its hydrogen envelope. Such an envelope is consistent with models of stripping at low metallicities (Klencki et al. 2022). Ramachandran et al. infer that the formation of a helium-rich star in SMCSGS-FS 69 was possible either via case A mass exchange or very early case B mass exchange, and point out several further candidate HeS stars in the Large Magellanic Cloud (LMC, $Z \approx 0.5 Z_{\odot}$).

Drout et al. (2023) measured UV-magnitudes of $\approx 500\,000$ stars in the direction of the LMC and SMC galaxies and selected 25 stars that may be binaries harboring HeS stars. Ten of these were spectroscopically analysed by Götberg et al. (2023) who determined their effective temperatures, $T_{\text{eff}} \sim (50\,000\text{--}100\,000)$ K, and bolometric luminosities, $L/L_{\odot} \sim (10^3\text{--}10^5)$. Surface gravities of the stars are $\log(g) \approx 5$, while hydrogen abundance in their atmospheres (by mass) does not exceed 0.4. These characteristics are compatible with those expected for $(1\text{--}8) M_{\odot}$ HeS stars.

Furthermore, as a possible explanation for the composite spectrum of the binary VFTS 291 in the 30 Dor complex in the LMC, Villaseñor et al. (2023) suggested that the binary contains a $(2.2 \pm 0.4) M_{\odot}$ HeS star, which is bloated due to instabilities in the He-burning shell. If true, this object must be quite unique, since stars spend less than 1% of their total nuclear-burning lifetime in this stage.

A systematic study of theoretical HeS star populations aimed at determining spectral and photometric characteristics along a sequence of increasing masses was performed by Götberg et al. (2018). This study renewed the general interest in the topic; however, it was limited to the products of a rather early case B mass exchange. In this work, only one model HeS star with a core He-abundance of 0.5 was selected from each evolutionary track with a given initial combination of ZAMS masses of components. The initial ratio of the primary and secondary masses (M_1, M_2) was fixed to $q_0 = M_2/M_1 = 0.8$. Furthermore, a single value of the initial orbital period was considered. Götberg et al. (2018) highlight the importance of recipes prescribing the mass-loss rate by radiatively driven stellar winds for the evolution and spectral appearance of the HeS stars. It should be noted however that their calculations were anchored to the empirically derived mass-loss rate of the qWR component in HD 45166, which is by now known to be spurious (Shenar et al. 2023).

In the present study, we computed an extended grid of binary stellar evolutionary models, leading to the formation of objects that could be identified with HeS stars, if observed. For the first time, we studied the entire range of combinations of the primary and secondary masses (M_1, M_2) and orbital period (P_{orb})

¹ See Hamann et al. (2019) and Sander et al. (2019) for the latest compilation of mass estimates of Galactic WR stars based on the evolutionary tracks for single rotating stars with $Z = 0.014$ (Ekström et al. 2012).

² Live “Galactic WR Stars Catalog” <http://pacrowther.staff.shef.ac.uk/WRcat>

³ Among the objects listed by Wang et al. (2023) as sdO-stars, the most massive $(2.4 \pm 0.5) M_{\odot}$ is the subdwarf component of γ Cas-type system π Aqr. However, most recently, Tsujimoto et al. (2023) classified this object as a WD and estimated its mass as $(0.51 \pm 0.01) M_{\odot}$. Gies et al. (2023) suggest that compact objects in the γ Cas-type subgroup of Be-stars are, actually, not sdO-stars, but WDs. Actually, the cumulative distribution of the sdB masses determined by combining the spectroscopic analysis with the fit of the SED and *Gaia* parallaxes becomes saturated at $M \approx 0.6 M_{\odot}$ (Schaffenroth et al. 2022). This may point to a different origin of the “low”- and “high”-mass subdwarfs.

on ZAMS that could produce binaries containing HeS stars. We determined the fundamental stellar parameters and the surface helium to hydrogen abundance ratios for the HeS stars, as well as for their companions. This allowed us to accomplish a population synthesis for binaries harboring $(1\text{--}7) M_{\odot}$ HeS stars in the Galaxy, and to evaluate their number and distributions over different parameters. In a subsequent paper, we plan to use the Potsdam Wolf-Rayet (PoWR) non-LTE code (e.g., [Hainich et al. 2019](#)) to produce synthetic spectra of binaries containing HeS stars, with the goal of enabling informative searches of binaries with HeS stars and/or explaining the selection effects precluding the detection of these systems.

The paper is organized as follows. In Sect. 2, the model and its assumptions are introduced. Section 3 describes the results of the model's calculations, while the discussion of the obtained results and our conclusions are presented in Sect. 4. In the appendices we display the test results, assuming alternative mass-loss prescriptions.

2. The model

2.1. Hot stripped helium stars

Our goal was to find HeS stars with masses bridging the gap between sdO/B and WR stars. To achieve this, we computed a grid of models of interacting binaries with the primary masses on ZAMS in the range $M_{1,0} \in [3\text{--}28] M_{\odot}$, the initial mass ratios of the components, $q_0 = M_{2,0}/M_{1,0} = 0.6, 0.8, 0.9$, and initial orbital periods between two days to several hundred days (depending on the masses of components and the initial q_0). In the systems with $q_0 < 0.6$ the components were expected to merge at RLOF stages; see below. However, we made several test runs for binaries with $q_0 = 0.4$ and found that in some cases the merger may be avoided.

As the first step, we defined the range of stellar parameters of binaries that allows us to identify stellar remnants after RLOF as HeS stars. We considered two values of the lower mass limit of HeS stars – $1 M_{\odot}$ and $2 M_{\odot}$ – in order to also address the scarcity of the observed “heavy” subdwarfs. The upper mass limit of HeS stars was taken as $7 M_{\odot}$, following [Nugis & Lamers \(2000\)](#), which is similar to the lowest mass estimate of the Galactic WR stars belonging to the nitrogen spectral subsequence (WN) obtained by [Hamann et al. \(2019\)](#). In our models, the luminosity of a stripped $7 M_{\odot}$ He star in the He shell burning stage corresponds to that of a star with a ZAMS progenitor mass close to $24 M_{\odot}$ and agrees also with the lower limit of the luminosities of Galactic, spectroscopically identified WN stars $\log(L/L_{\odot}) \approx 4.9$ (see Fig. 3 in [Shenar et al. 2020b](#)). This sets an upper mass limit of primary components of the models of close binaries in our computations. However, we also made several runs for binaries with masses up to $28 M_{\odot}$.

The considered temperature range was limited to the “hot” objects, with $\log(T_{\text{eff}}) \geq 4.4$, similar to T_{eff} of sdO/B subdwarfs. It should be noted that the stars occupying the uppermost part of the main sequence are hotter (see Figs. 3 and 4 in Sect. 3).

In this paper, we considered only one channel for the HeS star formation – a stable, nonconservative mass transfer in close binaries. This meant that we omitted other possibilities for the formation of HeS stars, such as a merger during a common envelope or the survival of the progenitor of a HeS star in common envelopes. All these scenarios have too many additional free parameters while hardly increasing the number of Galactic HeS stars.

2.2. Model assumptions

For the computations of the evolutionary tracks, we used the code MESA ([Paxton et al. 2011, 2013, 2015, 2018, 2019](#)), release 12778. Computations were performed for the metallicity $Z = 0.02$. We applied physical assumptions in the code that are similar to those used by [Sravan et al. \(2020\)](#) in their study of SN IIb progenitors. In the case of close binaries experiencing case A mass exchange, we accounted for rotation-induced mixing following [Sen et al. \(2022\)](#).

Unlike [Sravan et al. \(2020\)](#), we did not assume fixed values for the accretion efficiency but instead treated the mass and angular momentum loss from the system as regulated by the critical rotation of the accretor ([Packet 1981](#)). We assumed that the mass transfer through the vicinity of the L_1 point is conservative up to the instant when the initially nonrotating accretor attains a critical equatorial rotational velocity. After that, the accretion rate is limited by the amount of matter that corresponds to the critical rotation of the accretor, while the excess of the accreting matter leaves the system taking away the accretor's specific angular momentum. This is a kind of a “standard” scenario of the formation of HeS stars in binaries elaborated also by N. Langer and his coauthors (e.g., [Langer et al. 2003; Petrovic et al. 2005; Sen et al. 2022](#)) and applied, for instance, by [Yoon et al. \(2010, 2017\)](#) in studies of the progenitors of core-collapse SNe and by [Götberg et al. \(2017\)](#) in computations of models of stripped stars. The resulting evolution is completely conservative in the sense of mass and angular momentum before the rotation of the accretor becomes critical, but becomes almost nonconservative in mass and angular momentum later⁴.

The main-sequence companions of the nascent HeS stars become rapidly rotating and may be identified with Be-stars ([Kriz & Harmanec 1975; Pols et al. 1991](#); see also [El-Badry et al. \(2022\)](#) and references therein). This mechanism is consistent with the apparent deficiency of main-sequence companions to Be-stars due to a large difference in visual magnitudes and the difficulty of discovering subdwarf companions of Be-stars in UV ([Bodensteiner et al. 2020](#)). As El-Badry et al. claim, 10 to 60% of all Be-stars may be formed via this mechanism.

Other most critical assumptions concern the treatment of stellar winds. For $T_{\text{eff}} \leq 10\,000$ K and the surface hydrogen abundance, $X_{\text{s}} \geq 0.4$, we followed the prescription of [de Jager et al. \(1988\)](#) incorporated in MESA for the mass-loss rates over the HR-diagram scaled by $(Z/Z_{\odot}) = 0.85$ to match the Z-scaling of [Vink et al. \(2001\)](#). The wind mass-loss recipe from the latter paper was used for $T_{\text{eff}} \geq 11\,000$ K. For $10\,000 \text{ K} \leq T_{\text{eff}} \leq 11\,000$ K, the mass-loss rates were obtained by interpolation. For $T_{\text{eff}} \geq 11\,000$ K and $X_{\text{s}} \leq 0.4$ we used the mass-loss rates from [Nugis & Lamers \(2000\)](#).

The formation of HeS stars in case A mass exchange deserves special consideration. The relative number of stars subject to case A mass transfer is small, but not negligible, because the initial distribution of binaries over the logarithm of orbital periods is taken flat. Donors of the most tight binaries can experience mass-loss on the main sequence. The components of these binaries are rapid rotators due to tidal effects synchronizing the orbital and axial rotation. The velocities of the axial rotation in the systems with $P_{\text{orb},0}$ equal to a few days may amount to several 100 km s^{-1} . The rapid rotation induces

⁴ Efficiency of accretion is uncertain, but, definitely, small. In [Yoon et al. \(2017\)](#) the authors set efficiency of accretion to 20%. This causes slight difference of the masses of the RLOF remnants compared to the ones obtained in the present paper, where efficiency varies around 5%–7%.

a number of instabilities that result in the redistribution of the angular momentum and chemical species inside the stars (see Heger et al. 2000; Heger & Langer 2000). When accretion starts, the rotational velocity increases because of the angular momentum carried by the accreted matter. In order to treat more accurately case A mass exchange, we computed the evolution for this case following Sen et al. (2022), who took the effects of mixing into account⁵. Some systems experiencing case A mass exchange then avoid merging in the main-sequence and may produce HeS stars. Since the most rapidly rotating stars are components of low-mass tight binaries, the main effect of the case A evolutionary path is an increase in the number of low-mass He stars with masses overlapping with the mass range of “canonical” sdB/O stars, below $1 M_{\odot}$ and extending to $(4\text{--}5) M_{\odot}$.

Close binaries that experience case B mass exchange avoid merging, unless the initial binary mass ratio is $q_0 \lesssim 0.6$.

2.3. Population synthesis and cut factors

In the population synthesis, we assumed a Galactic star formation rate, $\text{SFR} = 2 M_{\odot} \text{ yr}^{-1}$ (Chomiuk & Povich 2011; Licquia & Newman 2015), the Salpeter IMF for the primaries of the initial systems, $dN/dM \propto M^{-2.35}$ between $0.1 M_{\odot}$ and $100 M_{\odot}$, a flat distribution over mass ratios of components on ZAMS, $q_0 = M_{2,0}/M_{1,0}$, and a flat distribution over $\log(P_{\text{orb},0})$ (Öpik 1924; Popova et al. 1982). The binarity rate was taken to be 50% (i.e., 2/3 of stars are in binaries). Under these assumptions, the number of binaries born annually in the Galaxy is $B \approx 1.14 \text{ SFR}/M_{\odot}$.

A detailed study of the $(3\text{--}28) M_{\odot}$ range of masses of primaries in close binaries with different mass ratios of components and orbital periods at ZAMS shows that not all stars in this mass range, in which the H shell burning layer is the main source of the energy release, in other words subject to case B mass exchange, really contribute to the formation of HeS stars via the RLOF. There are several “guillotine” factors.

(i) If the initial system is tight enough, the rejuvenation of the accretor, by bringing accreted matter into the core of the star (Kippenhahn & Meyer-Hofmeister 1977), which leads to an increase in the stellar radius, results in contact between the components and, most probably, the eventual formation of a rapidly rotating single star (e.g., de Mink et al. 2011; Menon et al. 2021). In case A mass exchange, this may happen even in the stage when the former donor contracts to high temperatures, but the former accretor is still a main-sequence star.

(ii) If the star fills its Roche lobe while it has a deep convective envelope, the mass-loss proceeds in the dynamical timescale and leads to the formation of a common envelope, which may result in the merger of the components or the formation of a tight binary system. In addition, if $q \lesssim (0.4\text{--}0.6)$, even if the envelope is radiative, the mass-loss typically occurs on a dynamic timescale and leads to the formation of a common envelope. Modeling of common envelopes requires 3D computations. All attempts to compute the evolution of CE-systems have thus far been unsuccessful, since a lot of processes occurring on different timescales are involved (see, e.g., Ohlmann et al. 2016; Gagnier & Pejcha 2023). Thus, there is an upper limit for the range of ZAMS periods of the potential precursors of HeS stars of several 100 days and a lower limit for q_0 (see Fig. 1).

In conventional population synthesis, the outcome of evolution in common envelopes is treated using the so-called

“common envelope efficiency” and the binding energy of the donor envelope (Webbink 1984; de Kool 1990). These parameters are highly uncertain (e.g., Ivanova et al. 2013). We discarded systems that pass through the common envelope stage and, therefore, they were “lost” in our modeling as binaries with HeS stars. We crudely estimated that the fraction of the “lost” binaries may comprise $\approx 10\%$ of the total population of HeS stars.

(iii) If the potential donor in a close binary is massive enough to ignite He in nondegenerate conditions, it may happen that, when it fills the Roche lobe between the terminal age main sequence (TAMS) and the base of the red giant branch in HRD, the mass of its He-core (in fact, only slightly less massive than the future HeS star) still does not exceed $\approx (1\text{--}2) M_{\odot}$ (Fig. 1). Observationally, the remnant will probably be identified as a subdwarf. This sets a lower limit on the HeS stars’ progenitor masses $(5\text{--}7) M_{\odot}$, depending on the initial orbital period (Figs. 1–4). This limit is slightly lower than $M_{1,0,\text{min}} \approx 7 M_{\odot}$, obtained by Götberg et al. (2018) for $q_0 = 0.8$ and a very early case B.

(iv) Stars more massive than $\approx 15 M_{\odot}$ continue to expand after He ignition in nondegenerate cores and can still fill critical lobes. Later, the contraction that accompanies He-burning terminates RLOF after a fraction of the H/He envelope has been lost, but a relatively large fraction of it is still retained. Then the star may continue to burn He in the core close to the RG branch to become a red supergiant with a CO core. In some cases, it may refill the Roche lobe. But when the mass-loss terminates and the star contracts, because of the presence of a relatively massive H/He envelope, it never becomes cool enough ($\log(T_{\text{eff}}) \leq 4.4$) to be considered in this study as a HeS star. We looked into the evolution of such stars and found, as expected, that the remnants of these stars are massive enough to experience a SN explosion. Depending on the amount of H and He retained in the envelope, despite the stellar wind and mass-loss in the loops of their tracks in the HRD, such SNe may be classified as Ib or IIb.

Thus, a fraction of the deemed progenitors of binaries with HeS stars may be lost. The progenitors of hot helium stars with masses between those of subdwarfs ($\lesssim 2 M_{\odot}$) and WR stars ($\gtrsim 7 M_{\odot}$) are not binaries with $M_1 \gtrsim 2.5 M_{\odot}$, as is often claimed, but objects with $M_{1,0}$ at least 2.5–3.5 times higher and with a limited range of ZAMS periods and mass ratios. This reduces their relative number compared to the subdwarfs and WR stars.

3. Results of computations

3.1. Initial-final mass relation for progenitors of HeS stars and orbital periods of the binaries with HeS stars

Figure 1 shows the full grid of computed models in the systems with initial mass ratios of components, $q_0 = M_{2,0}/M_{1,0} = 0.6, 0.8, 0.9$ in the diagram $M_{1,0}$ versus P_0 . For binaries with $q_0 < 0.6$, mass exchange is, as a rule, unstable. Nevertheless, some systems with $q_0 = 0.4$ avoid components merging and produce $2 M_{\odot}$ to $7 M_{\odot}$ HeS stars with $3.5 M_{\odot}$ to $7.5 M_{\odot}$ companions (see Fig. 7 below).

The masses of stripped stars for the analysis are taken at the positions along the tracks where the luminosity reaches its minimum. Close to these points, HeS stars spend most of the core He-burning time, which is $\sim 10\%$ of the main-sequence lifetime. Figure 1 also shows the “fate” of the binaries.

The positions of colored regions in the left panel of Fig. 1 illustrate the effect of the “guillotine” factors that define which ZAMS binaries may produce HeS stars via stable nonconservative mass exchange, as discussed above in Sect. 2.3.

⁵ Note that in the latter paper the diffusion coefficients describing the rotation-induced instabilities have the maximum values.

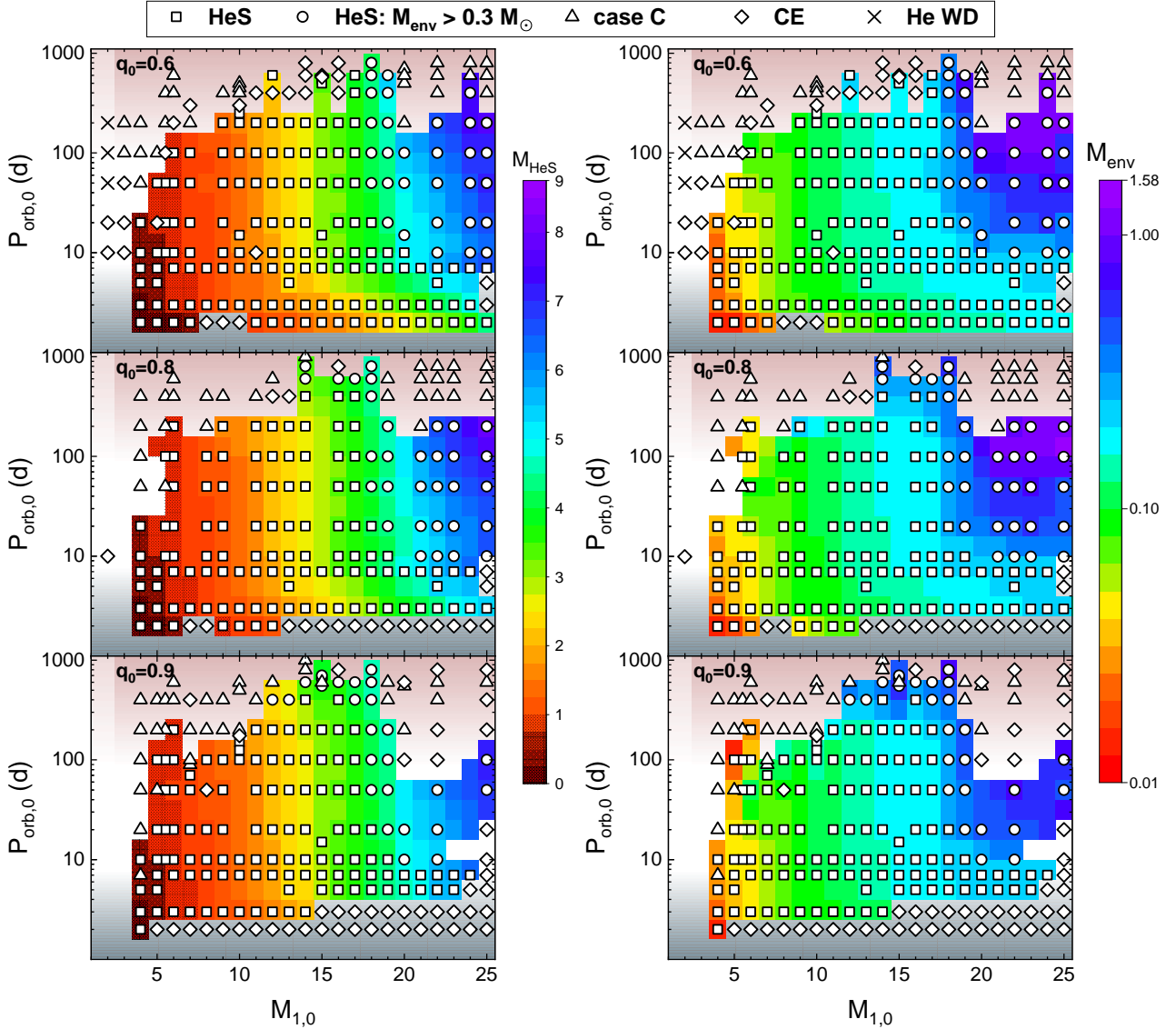


Fig. 1. Grid of computed systems. Left panel: models of binaries with initial mass ratios, $q_0 = M_{2,0}/M_{1,0} = 0.6, 0.8, 0.9$ in the “ZAMS mass of the primary component, $M_{1,0}$ – initial orbital period, $P_{\text{orb},0}$ ” plane. Color-coded are the masses of the remnants of primary components of the binaries after RLOF at the point of the lowest luminosity along the post-mass-exchange evolutionary track, obtained by a numerical approximation of the results of the computation of a non-regular grid of models. The legend over the upper panel shows the evolutionary “fate” of the computed binaries. Open squares and circles indicate the formation of HeS stars (in the latter case, with retained H/He envelopes exceeding $0.3 M_{\odot}$). The diamonds show binaries entering common envelopes. Open triangles stand for binaries where case C mass transfer occurred. In the light gray region at the top left of the middle and lower panels, the models for $q_0 = 0.9, 0.8$ were not computed, since binaries in this region definitely experience case C mass transfer and form common envelopes, or the T_{eff} of the stripped component never exceeds 25 000 K. Crosses mark the systems forming He WDs. The “pixels” overplotted by dots show the locations of the progenitors of stripped helium remnants with masses $< 1 M_{\odot}$. Right panel: color-coded masses of H/He envelopes retained by the remnants of the initial primary components shown in the left panel at L_{\min} along their tracks (with steps $0.01 M_{\odot}$ and $0.1 M_{\odot}$ below and above $M_{\text{env}} = 0.1 M_{\odot}$ respectively). All masses are in M_{\odot} .

The systems with masses of the H/He envelopes of remnants exceeding $0.3 M_{\odot}$ (open circles) are highlighted because, if the remnants retain such a mass of the envelope after the He-burning stage, they do not expand after the core He-exhaustion and do not lose mass due to the refilling of critical lobes.

The masses of envelopes, as well as the masses of HeS stars, are to some extent uncertain, because after cessation of RLOF they decrease by the stellar wind as stars evolve toward higher T_{eff} . Masses of envelopes (and masses of HeS stars) in the core He-burning stage may remain almost the same if Vink (2017) stellar wind mass-loss is used, or decrease by several $0.1 M_{\odot}$ if Nugis & Lamers (2000)’s law is applied. The figure shows that

the star may become really “naked”, virtually without any hydrogen at the surface. Since we applied Nugis & Lamers’ recipe, this possibility is quite realistic (see also Figs. 2, A.1, and B.1). However, it should be noted that the issue of a “correct” mass-loss rate law is not solved as of yet.

Figure 2 shows “ZAMS mass – remnant mass” and “remnant mass – envelope mass” relations for the HeS stars produced by the systems from the grid of initial systems. Like in Fig. 1, the masses of HeS stars and their envelopes are shown for the lowest luminosity point along the evolutionary track, where helium stars spend most of their lifetime. A feature seen both in Figs. 1 and 2 is a quite weak dependence of HeS star

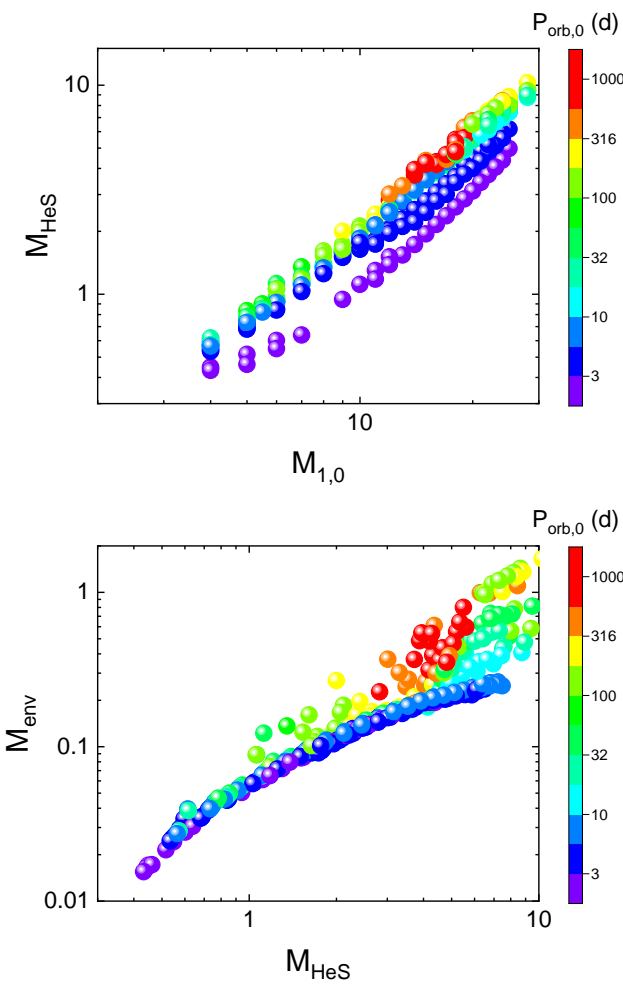


Fig. 2. ZAMS mass – remnant mass (upper panel) and remnant mass – H/He envelope mass (lower panel) relations for the HeS stars produced by the systems from the grid of initial systems. Color-coded are ZAMS periods of the binaries. All masses are in solar units.

masses on $P_{\text{orb},0}$. The reason for this is that there is only a small change in He-core masses during the rapid crossing of the Hertzsprung gap. Stars with $M_{\text{HeS}} \geq 2 M_{\odot}$ in the stable nonconservative mass-exchange channel are produced only by binaries with $P_{\text{orb},0} \gtrsim 10$ days and masses $\gtrsim (10-12) M_{\odot}$. Moreover, it is clear that for $M_{\text{HeS,min}} = 1 M_{\odot}$ the lower limit of the progenitor masses is close to $6 M_{\odot}$, while the initial orbital periods should exceed two to three days. However, the remnants of stars with $M_{1,0}$ slightly below $6 M_{\odot}$ may also spend some short time in the HeS stars' domain of the HRD during the shell helium burning, as illustrated below by the track for a star with a ZAMS mass of $5 M_{\odot}$ in Figs. 3 and 4 (the lower dotted track).

Generally speaking, the outcome of the evolution and masses of HeS stars rather weakly depends on the initial mass ratio q_0 . This is related to a very weak dependence of the radii of critical lobes on q_0 . For a given $M_{1,0}$ and $P_{\text{orb},0}$, $R_{\text{cr}} \propto (1+q)^{-1/3}$. Noticeable as well is a slightly steeper increase in masses of HeS stars with an increase in $M_{1,0}$, as q_0 decreases.

3.2. Synthesized HeS stars and their progenitors in the HRD

In Fig. 3 we present the relative positions of some of the computed HeS stars and their progenitors in the HRD. We mark with similar colors the progenitors of HeS stars (crosses) and their

descendants (circles) in order to show their relative displacement in the HRD. In this figure and in Fig. 4, the domains occupied by HeS stars and their progenitors and by the Galactic WN stars according to Shenar et al. (2020b, in the upper left corner of the plot) are outlined with dashed magenta lines.

In the low T_{eff} part of the HRD, the domain of progenitors for stars less massive than $15 M_{\odot}$ is limited by the core He ignition line, since the latter causes overall contraction of stars. For more massive stars, the low T_{eff} limit is due to high mass-loss rates resulting in the formation of common envelopes or the formation of mass-loss remnants with relatively massive H/He envelopes that contract but that do not reach the $T_{\text{eff}} = 25\,000$ K required to classify them as HeS stars, as was explained above. Additionally, there are stars in which RLOF occurs close to the Hayashi line but is terminated after only a part of the envelope is lost, because He-burning becomes the dominant energy source. These stars continue their evolution as red supergiants.

Figure 3 shows some of the computed models of HeS stars at the positions where their luminosity along the tracks reaches its minimum. Close to these points, HeS stars spend a fraction of the core He-burning time when they have the core He abundance ≈ 0.5 . The rest of the core He-burning occurs when the stars evolve to higher luminosities and T_{eff} . In the latter stage, T_{eff} may increase by $\Delta(\log(T_{\text{eff}})) \approx 0.05$, while $\Delta(\log(L/L_{\odot}))$ may be up to 0.5, as is seen for the tracks plotted in Figs. 3 and 4. The time spent in the “ascending” branch of the track is comparable to the time spent around the luminosity minimum. These core He-burning stars create a subpopulation of HeS stars on the hot side of the strip of stars with minimum luminosity during the core-He burning stage, which is clearly seen below in Fig. 6.

In addition, we plot in the diagram the track of an $M \approx 0.7 M_{\odot}$ remnant of a $5 M_{\odot}$ star (the lower dotted line) that enters the domain of HeS stars only for a very short time in the stage of contraction, when an H shell still dominates in luminosity and during He shell burning (the part of the track turning up at $\log(T_{\text{eff}}) \approx 4.6$ and then leftward). The He shell burning is unstable, and the track makes loops in the HRD, a part of which extends beyond the left limit of the plot.

In this figure, the track of a $22 M_{\odot}$ primary star in the system with $q_0 = 0.6$ is a kind of “limiting” one for the systems experiencing case A mass exchange. The core He-burning of more massive stars occurs in the WR-stars domain of the HRD. For case B, this limiting mass is $24 M_{\odot}$.

Figure 4 displays the positions of HeS stars and their progenitors in the HRD. It is clear that the population of HeS stars is distinct from the population of “canonical” subdwarfs and is bridging locations of sdO and WR stars in the HRD. This is in agreement with the results of Götberg et al. (2018), which suggest that subdwarfs, HeS, and WR stars form a continuous spectral sequence where the strength of the He II $\lambda 4686$ Å line increases from absorption to emission.

Both Figs. 3 and 4 suggest that the population of HeS stars is dominated by low-mass objects ($\lesssim 4 M_{\odot}$) for a wide range of ZAMS masses up to $\approx 15 M_{\odot}$. This reflects the initial mass function of the primary components of binaries and variation in the range of He-core masses. It is noteworthy to mention that in the HRD the domain of the most massive HeS stars ($M_{\text{He}} \gtrsim 5 M_{\odot}$) overlaps with the location of the main-sequence stars more massive than $\sim 10 M_{\odot}$. There is a kind of gap in the HRD at $\log(T_{\text{eff}}) \approx (4.0-4.4)$ and $\Delta(\log(L/L_{\odot})) \approx (2.5-4.2)$. It is populated by the stars that are not hot enough to be classified as HeS stars but that have He-enriched envelopes.

Figures 3 and 4 indicate that the formation of massive sdO-stars ($1-2 M_{\odot}$) may be explained if they descend

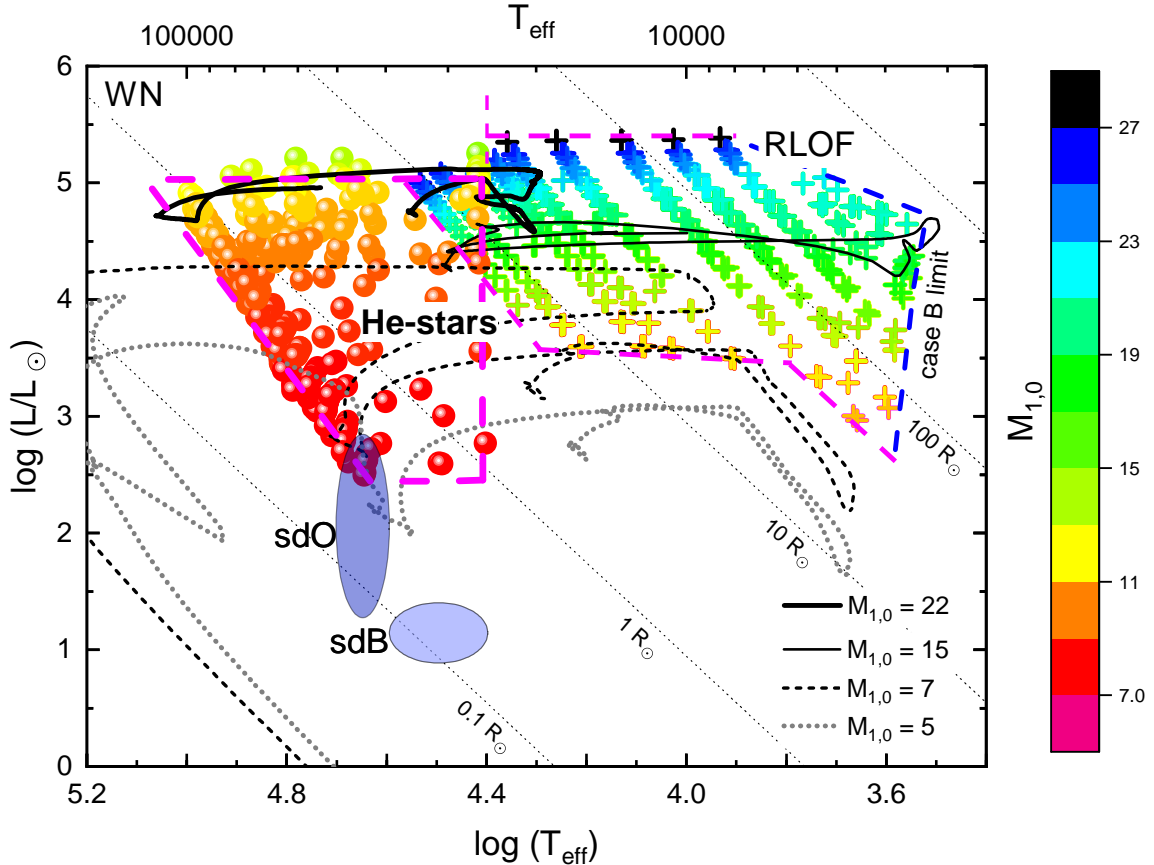


Fig. 3. Positions of HeS stars (at the minimum luminosity along their evolutionary tracks, see the text) and their progenitors in the HRD. The ZAMS masses are color-coded. The crosses mark the progenitors of HeS stars at the beginning of the RLOF, and the filled circles show HeS stars descending from them. The progenitor's and descendant's symbols of the same color belong to the same evolutionary tracks, i.e., red circles denote the descendants of red crosses, yellow circles the descendants of yellow crosses, and so on. Dashed magenta lines bound the regions occupied by the Galactic WN stars, HeS stars, and precursors of the latter. In the upper right corner, dashed blue lines indicate the limits of case B mass exchange and stable quasi-conservative mass exchange. The black symbols in the diagram indicate stars with ZAMS mass $28 M_{\odot}$, which produce WR stars. Thick and thin solid and dashed lines show the evolutionary tracks of the primaries of binaries with ZAMS masses of 22, 15, and 7, and $5 M_{\odot}$, and initial periods of 5 (case A mass exchange), 550 (case B), 100 (case B), and 50 days (case B), respectively, illustrating the formation paths of HeS stars. The thin dotted lines are the lines of equal stellar radii. The gray ellipses depict the locations of sdB and sdO-stars (from Heber 2016, Fig. 1).

from the stars with ZAMS masses $\approx(5-10) M_{\odot}$, in contrast to the canonical $\sim 0.5 M_{\odot}$ subdwarfs with progenitor masses below $2 M_{\odot}$ (Iben & Tutukov 1985; Han et al. 2002, 2003; Yungelson & Tutukov 2005). Interestingly, Fig. 4 shows that known massive sdO companions of Be-stars (Wang et al. 2023) may be either in the core or shell He-burning stage.

3.3. Synthesized Galactic HeS population properties

Figure 5 shows differential and cumulative distributions of the formation rate and the total number of binaries containing HeS stars. For the limiting mass of HeS stars, $M_{\text{lim}} = 1 M_{\odot}$, their formation rate is only about 1/170 yr and their number in the Galaxy is close to 19 500. If $M_{\text{lim}} = 2 M_{\odot}$, the formation rate and number of HeS stars sharply decrease to about 1/360 yr and 3100, respectively. The dominance of low-mass HeS stars, actually overlapping with the mass range of the most massive sdO-stars, is clearly seen.

The HRD of the synthesized population of HeS stars is shown in Fig. 6. We note the absence of colored circles in the leftmost part of the shaded region. This is because we plot the positions of HeS stars in the HRD at the minimum luminosity,

in other words at an evolutionary stage where the stars spend a substantial fraction of their core He-burning time. However, a total exhaustion of He in the core occurs at a slightly higher luminosity (see captions to Figs. 3 and 4).

For the stars that make loops in the HRD in the He shell burning stage during which $\log(T_{\text{eff}})$ becomes lower than 4.4, we took into account the time spent by them before $\log(T_{\text{eff}})$ becomes lower than 4.4 for the first time. The remaining He shell burning time is short and can be safely neglected.

As can be seen in Fig. 6, the majority of HeS stars populate a rather narrow ($\Delta(\log(T_{\text{eff}})) \approx 0.2$) “strip” between $\log(T_{\text{eff}}) \approx 4.6$, $\log(L/L_{\odot}) = 2.5$ and $\log(T_{\text{eff}}) \approx 4.9$, $\log(L/L_{\odot}) = 4$. The objects located at a lower T_{eff} originate in binaries with relatively large ($\gtrsim 100$ days) initial orbital periods, which retain massive H/He envelopes and burn the core He at $T_{\text{eff}} < 25 000$ K, in other words below the limit we adopted for HeS stars.

There are relatively densely populated branches of $\approx 5 M_{\odot}$ HeS stars extending to a lower T_{eff} from the main “strip”. These are the descendants of binary components more massive than about $15 M_{\odot}$ that retained relatively massive H/He envelopes, but not exceeding $0.3 M_{\odot}$. The stars with more massive envelopes never reach $\log(T_{\text{eff}}) = 4.4$. We distinguish the latter as a

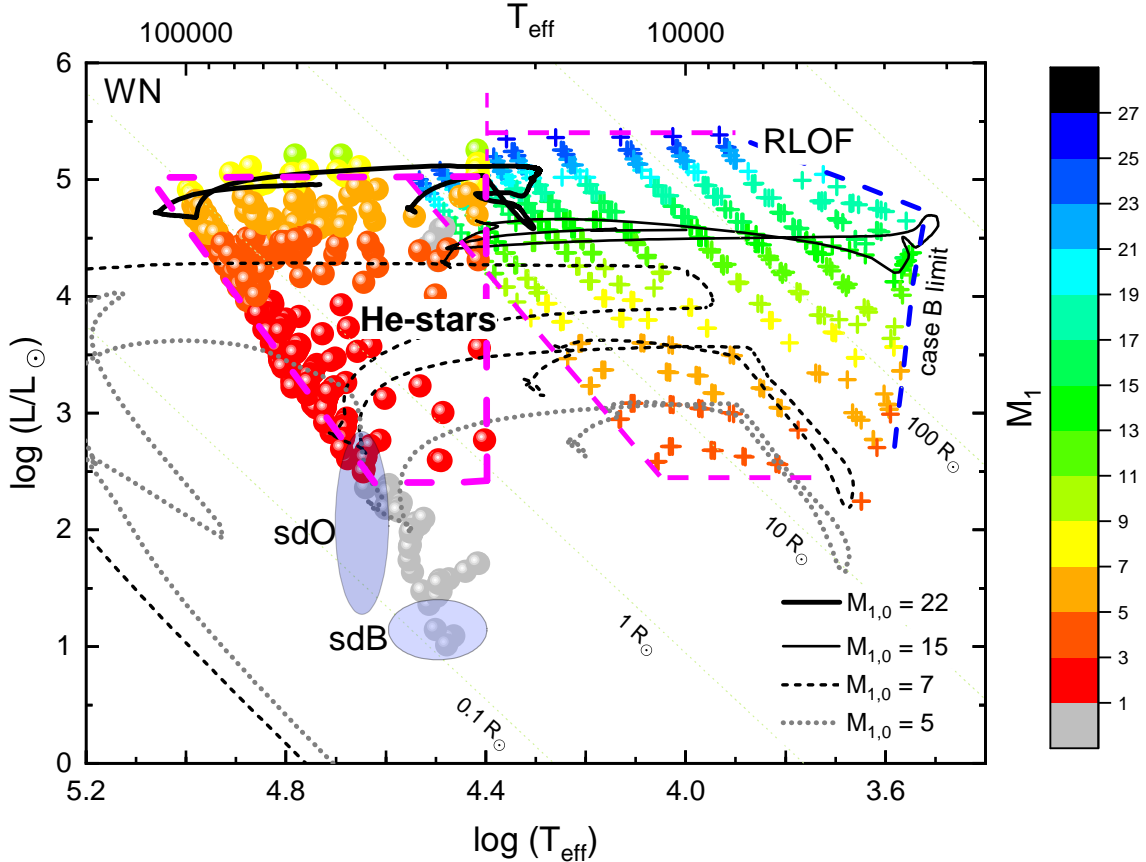


Fig. 4. Same as in Fig. 3, but the color scale encodes the stellar masses at the RLOF and in the core He-burning stage after the RLOF. The entire stage of He core-burning stretches from the position of the circles by about ± 0.05 in $\log(T_{\text{eff}})$ and up by $\lesssim 0.5$ in $\log(L/L_{\odot})$. Gray circles show the descendants of $(5-7) M_{\odot}$ ZAMS primaries producing HeS stars less massive than $1 M_{\odot}$ in case B mass exchange. Initial parameters of the 5, 7, 15, $22 M_{\odot}$ tracks shown in the plot are the same as in Fig. 3.

separate category of stars with He-enriched envelopes, as already mentioned in Sect. 3.3.

The most luminous among our synthetic population are WR stars (these are marked in black and three dark shades of blue in the upper panel of Fig. 6). The position of the most massive HeS stars overlaps with that of WR stars at $\log(T_{\text{eff}}) \approx (4.7-4.9)$ because HeS stars spend a short shell helium-burning time at high luminosities. But it is evident that such stars should be scarce. It is worth noticing that the remnants of case A mass exchange systems belong to the population with the highest T_{eff} and always burn He close to the minimum luminosity point of the track (see the lower panel in Fig. 6).

Figure 7 shows the masses of components of binaries in the synthesized population as a function of the initial mass ratio of components. The effective temperatures of stars have a weak trend, visible already in Fig. 4: the most numerous HeS stars with masses below about $3 M_{\odot}$ have the highest T_{eff} . In addition, the trend of the T_{eff} to decline with an increase in the HeS star mass is seen.

According to our assumptions about the mass and angular momentum loss (see Sect. 2.1), the mass of the accretor changes only by several percent. Therefore, the minimum masses of companions to HeS stars are very close to those in the model grid, that is, $4 M_{\odot}$, which corresponds to the spectral type B7V ($\log(L/L_{\odot}) \approx 2.5$, $T_{\text{eff}} = 14\,000$ K, Pecaut & Mamajek 2013).

It is suggested that HeS stars may be detected thanks to the excess of the UV emission of the binary hosting a HeS star

compared to the UV emission of a single star with a mass equal to the main-sequence mass of its companion (Götberg et al. 2018). We roughly plot in Fig. 7 the lines for two values of color excess (GALEX/NUV-SDSS/r), as computed by Götberg et al. Helium stars with companions that have masses below the limits shown by these lines may be detectable.

Figure 7 suggests that for the color excess $\lesssim 0.05$, in the absence of other selection effects, about 50% (≈ 1500) of the binaries hosting HeS stars more massive than $\approx 2 M_{\odot}$ (approximately, the mass of the most massive known sdO) are “detectable”. The other 50% are outshone in UV by their companions. As was shown by Götberg et al., using the excess in the emission line He II $\lambda 4686$ as a signature of the presence of a HeS star provides similar results. By no means is the number ≈ 1500 quoted above an upper limit for a potentially detectable population of HeS stars. Clearly, more dedicated work is needed to identify potential “smoking gun” spectral and photometric features of HeS stars in binaries. Such a study will be presented in a follow-up work.

Figure 7 also demonstrates several effects related to the initial mass ratio, q_0 . First, the range of M_{He} only slightly depends on the initial q_0 ; this is a consequence of the weak dependence of the radii of the critical lobes on q . Second, it confirms an increase in the steepness of the mass ratio of components in the systems harboring HeS stars (M_{He}/M_2) with an increase in the initial q_0 , as was seen already in Fig. 1. This is a direct result of the algorithm for mass and angular momentum loss from the

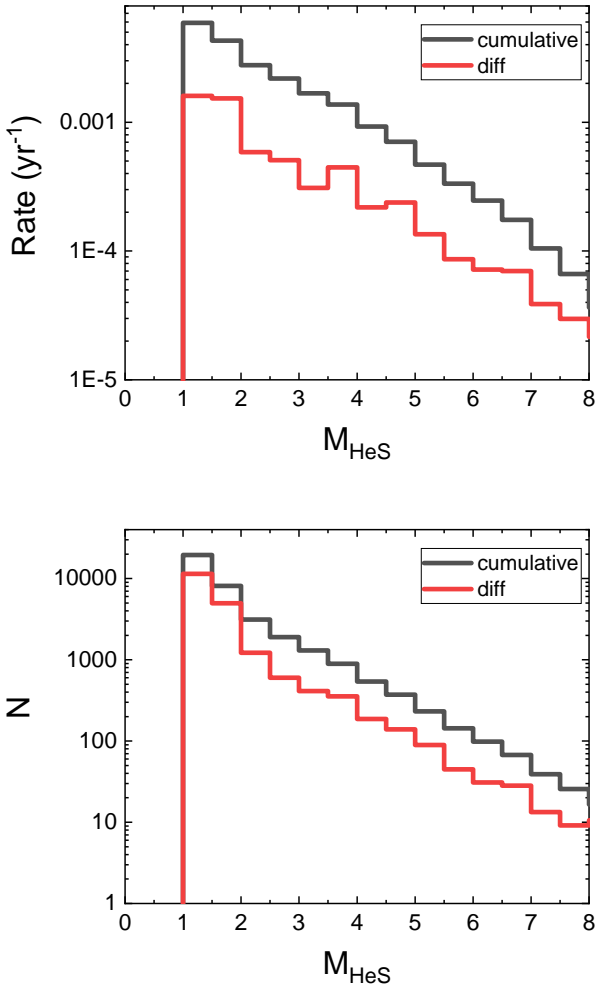


Fig. 5. Differential and cumulative distributions of the formation rate of HeS stars with masses $\geq 1 M_{\odot}$ as a function of the stripped star mass (upper panel). Differential and cumulative distributions of the total number of HeS stars in the Galaxy (lower panel).

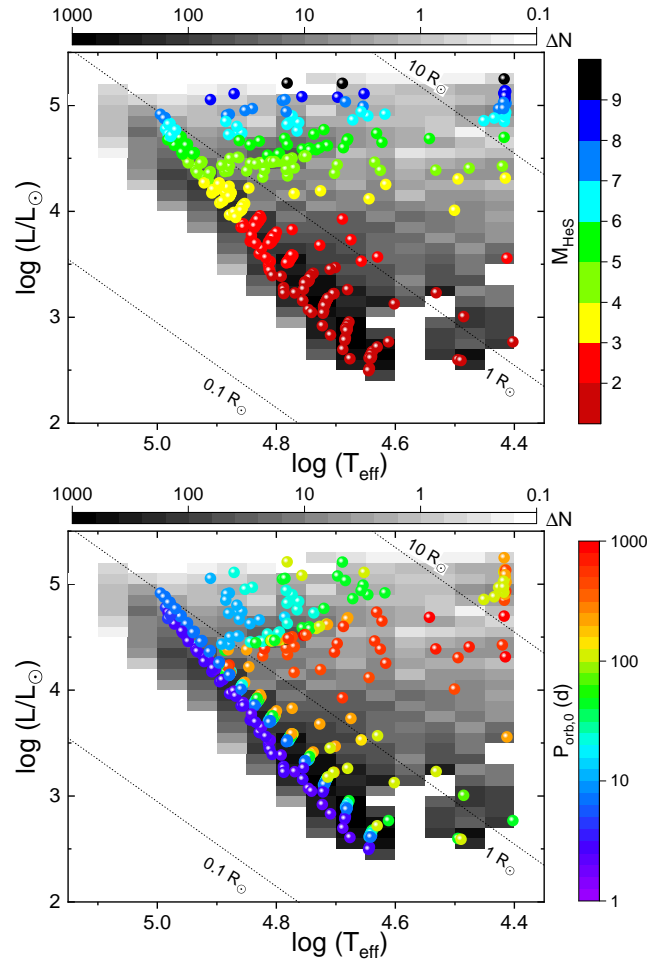


Fig. 6. HRD of the synthesized population of HeS stars. The gray scale shows the number of HeS stars per $\Delta(\log(T_{\text{eff}})) \times \Delta(\log(L/L_{\odot})) = 0.05 \times 0.1$ pixels. Upper panel: symbols are color-coded according to the HeS stars' masses (scale to the right). Lower panel: symbols are color-coded according to the initial binary periods. Circles mark the positions of the computed models, like in Figs. 3 and 4.

system, which strongly limits the amount of accreted mass by several percent of the initial accretor's mass. Finally, it shows that, as long as $q_0 \gtrsim 0.6$, both cases A and B of mass exchange enable the formation of HeS stars, within the primary ZAMS mass and orbital period limits outlined in Figs. 1, 3, and 4. Figure 7 suggests that a significant fraction of HeS stars with masses $(2-4) M_{\odot}$ are potentially detectable.

The relation between the luminosities of HeS stars (at the minimum luminosity in the core He-burning stage, L_{He} , as in other figures) and the luminosities of their companions, L_2 , at the same instant of time is shown in Fig. 8. As can be seen, L_{He} may be both lower or higher than L_2 depending on the HeS star's mass. Considering that bolometric corrections will favor the optical luminosity of main-sequence stars, one may expect that the majority of HeS stars will be outshone by their companions in the visual, while in UV the situation may be more favorable. But this could be confirmed only by computing bolometric corrections for both components. Since in the shell He-burning stage the luminosity of helium stars is higher than in the core He-burning stage, the former may be more favorable for the detection of HeS stars; however, its short duration acts in the opposite direction. We also show in this figure the relation $L_{\text{He}} - L_2$ for several systems descending from binaries with

$M_{1,0} = (5-7) M_{\odot}$, but not producing HeS stars more massive than $1 M_{\odot}$ (the gray symbols in Fig. 4).

Figure 9 shows the relation between the masses of HeS stars and the orbital periods of the binaries harboring them, overplotted over the distribution of the synthesized population. Colors code the $\log(T_{\text{eff}})$ of HeS stars. We note the absence of systems with $P_{\text{orb}} \lesssim 4$ days and larger than 5000 days. Most of the binaries have orbital periods ranging from 10 to 1000 days. The orbital periods do not correlate with T_{eff} . Both "hot" and "cold" HeS stars populate the same range of P_{orb} . The figure confirms the conclusions made before: the most massive HeS stars often have a low T_{eff} (within our assigned limit, $\log(T_{\text{eff}}) \geq 4.4$, for HeS stars) due to the presence of massive H/He envelopes. Remarkably, the range of P_{orb} of most systems is the same as the range of periods of their progenitor systems, below about 1000 days, see Fig. 1.

Figure 9 clearly suggests that a large P_{orb} is one of the factors hampering the discovery of HeS stars in binaries. Companions of HeS stars are rapidly rotating. As is noted by El-Badry et al. (2022), measurements of the radial velocity shifts of Be-stars are not reliable due to their high rotation velocities and disk-driven spectral variability. Therefore, measuring the orbital periods of binaries containing HeS stars is not easy. If taken at face value,

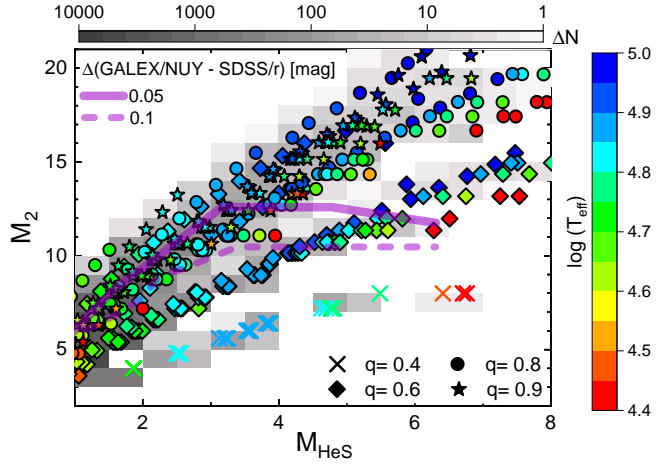


Fig. 7. Relation between masses of components in the synthesized population of binaries with HeS stars. Different symbols denote the descendants of binaries with different initial mass ratios of components, q_0 . The symbols are color-coded by the T_{eff} of HeS stars. The gray scale codes the number of stars per $\Delta(M_{\text{HeS}}) \times \Delta(M_2) = 1.0 M_{\odot} \times 1.0 M_{\odot}$ pixel. Solid and dashed magenta lines show roughly two limiting values of the UV color excess (GALEX/NUV-SDSS/r) computed by Götberg et al. (2018), below which HeS stars may be detected due to their color excess compared to the UV color of the companion (assumed to be a main-sequence star).

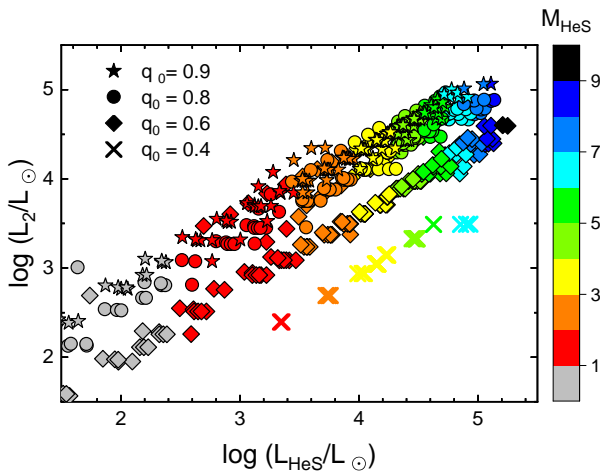


Fig. 8. Relation between luminosities of HeS stars and their companions in the computed binaries with different initial mass ratios (symbols in the insert). The gray symbols show systems that failed to produce HeS stars. The color scale codes the masses of HeS stars.

in the sample of known Galactic Be-stars with identified sdO companions, the orbital periods do not exceed ≈ 200 days.

The dependence of HeS star parameters on the effective temperature is presented in the left panel of Fig. 10. In the nHe/nH– T_{eff} diagram, two groups of stars can be seen. The upper, more populous group is formed by stars that overflow critical lobes at $P_{\text{orb}} \lesssim 100$ day. Initially wider systems are predominantly He-poor since they have heavier He-cores and less H-exhausted surface layers when RLOF terminates. The lower group includes stars that retained envelopes more massive than $0.3 M_{\odot}$; these stars form in binaries with the longest initial P_{orb} . The stars in this group are the most massive among the HeS star population. Actually, this plot reflects the fact that more massive stars need to lose relatively less matter in order to detach from critical lobes, as was noticed already in early papers on case B

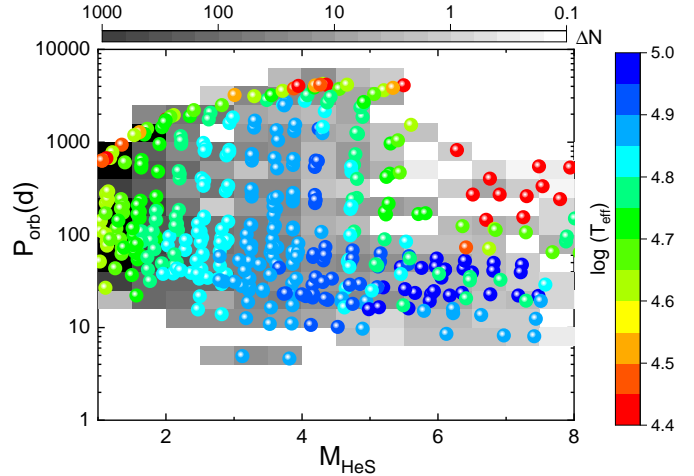


Fig. 9. Relation between HeS star masses and the orbital periods of binaries harboring them. The gray scale codes the Galactic number of stars per pixel. The color scale codes the effective temperatures of the stars.

evolution in massive stars (e.g., Tutukov et al. 1973). Compared to the sdB/O stars, the range of nHe/nH of HeS stars is much more narrow; for the former, its logarithm ranges from –4.0 to 3.0 (Heber 2016, Fig. 5).

The $\log(T_{\text{eff}})$ – $\log(g)$ diagram is also structured. Evidently, the most compact and massive stars have the largest surface gravities. There is a branch of stars stretching from a high g , high T_{eff} region to a low g , low T_{eff} region formed by relatively less massive HeS stars. This may be understood as an effect of RLOF at increasing periods, resulting in less compact HeS stars. The $\log(g)$ values of HeS stars are within a broad range from 5.5 to 2.5, while for sdB/O stars they fall inside the narrower (6.3–5.0) interval (Heber 2016, Fig. 5). This reflects a broader range of masses and radii of HeS stars compared to subdwarfs.

The right panel of Fig. 10 shows the distribution of masses of H/He envelopes retained by HeS stars at the lowest luminosity points along the evolutionary tracks in the synthesized population of HeS stars. Most HeS stars have low-mass envelopes with $-0.2 \lesssim \log(n\text{He}/n\text{H}) \lesssim 0.2$, and hence the envelopes of these stars are He-dominated. The profile of chemical abundances in the envelopes of nascent HeS stars is defined by several factors: the stellar mass at the RLOF termination, the profile of abundances in the star, and the stellar wind acting as the star moves to the high T_{eff} region of the HRD. More than half of HeS stars descend from low-mass progenitors, which have relatively massive H/He envelopes after the cessation of RLOF. In this case, the increase in nHe/nH is due to the mass-loss by stellar wind.

The rest of the stars have a wider range of envelope masses, up to almost $1 M_{\odot}$ in the most massive ones with a T_{eff} lower than 40 000 K. Though, in this group of stars also, the majority of objects have $M_{\text{env}} \lesssim 0.2 M_{\odot}$ (the darkest shades of the gray scale). A more scattered group of stars with $(0.2\text{--}0.4) M_{\odot}$ envelopes extending toward high T_{eff} are the remnants of more massive stars for which wind mass-loss is less significant because of a very fast evolution. The X/Y ratio range of about 0.3 to 0.5 is typical for the remnants of massive donors in close binaries.

The middle panel demonstrates an evident fact, that stars with low-mass envelopes are more compact, and hence have a higher $\log(g)$.

Finally, the HRD in the lower panel shows, again, a kind of compact sequence of descendants of low-mass (in the range

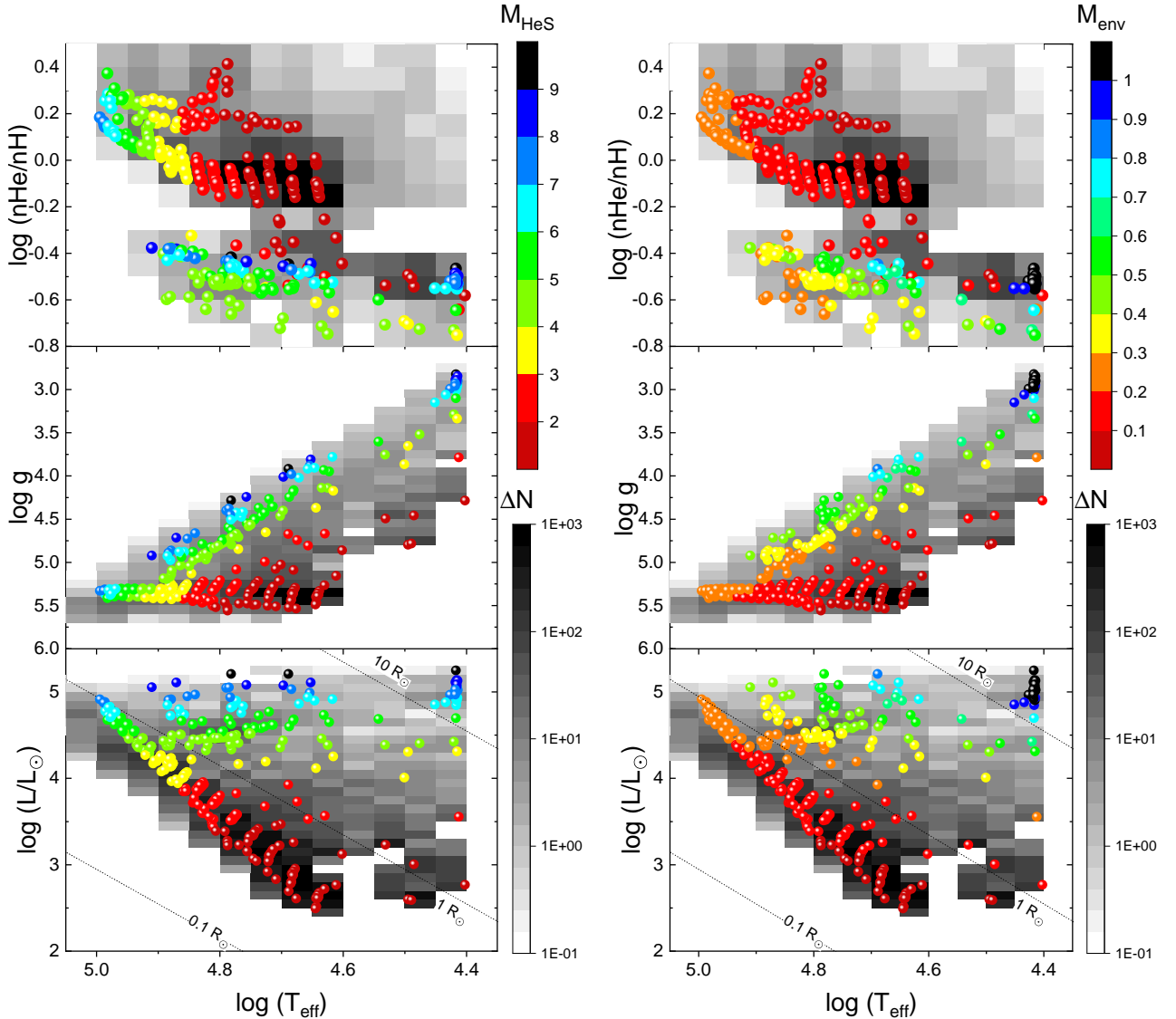


Fig. 10. Parameters of the synthesized population of HeS stars. Upper panel: distribution of the surface He-abundance ($n\text{He}/n\text{H}$); middle panel: log of surface gravity ($\log(g)$); lower panel: HRD. The symbols are the same as in Fig. 6. The gray scales in all panels show the Galactic number of systems per pixel. The colors in the left panels encode the masses of HeS stars, while the colors in the right panels encode the masses of H/He envelopes.

under study) stars with the least massive envelopes and a scattered population of stars with different envelope masses depending on the initial masses of HeS star progenitors. Remarkably, the most massive envelopes have HeS stars positioned in the HRD in the region close to $\log(T_{\text{eff}}) \approx 4.4$, where the domain of HeS stars and WR stars overlaps with the main sequence (Figs. 3 and 4).

4. Discussion and conclusion

In the present paper we have addressed the issue of the observed scarcity of Galactic hot helium stars (HeS) with masses in the range $(2-7) M_{\odot}$, that is, between the most massive sdO subdwarfs and WR stars. We have performed a population synthesis of such stars, based on evolutionary computations for a grid of close binary systems leading to the formation of HeS stars in this mass range, using the code MESA. We explored the full range of initial masses, orbital periods, and mass ratios of components of close binaries resulting in the formation of hot He stars in the

above-mentioned mass range (Figs. 1 and 7). In this sense, our investigation is more comprehensive than the studies that aimed at the same stars (Götberg et al. 2018) or at the formation of progenitors of core-collapse SNe that pass through the same evolutionary stage and have masses in the same range as HeS star progenitors, for example Yoon et al. (2017) and Sravan et al. (2020). We took into account rotation-induced mixing for the most tight binaries experiencing case A mass exchange.

The results of our population synthesis suggest that there can be several reasons for the apparent scarcity of HeS binaries in the Galaxy. In the first place, to form a HeS star, a stable mass transfer in a binary should occur, which is possible in restricted ranges of the initial orbital periods, P_0 , and binary mass ratios, q_0 , allowing the avoidance of a runaway mass transfer and common envelope formation. Our calculations enabled us to find the corresponding range of the initial binary systems' parameters (see Fig. 1). A detailed tracing of the evolutionary paths leading to the HeS stars' location in the HRD (Figs. 3 and 4) suggests that most of the Galactic HeS stars descend

from the initial binaries with ZAMS primary masses from $\approx 5 M_{\odot}$ to $\approx 24 M_{\odot}$.

The remnants of stars that stably lose mass via RLOF may still retain massive H/He envelopes and never become “hot” (they have $\log(T_{\text{eff}}) < 4.4$). For the assumed Galactic SFR = $2 M_{\odot} \text{ yr}^{-1}$, our systematic exploration of the entire range of possible progenitors of He-stars with masses greater than $1 M_{\odot}$ resulted in a Galactic number of HeS stars close to 20 000 or about 3000, if their mass exceeds $\sim 2 M_{\odot}$ – the mass of the most heavy subdwarfs (Fig. 5).

Götberg et al. (2018) evaluated the fraction of Galactic early B- and O-stars hiding HeS stars companions as $\sim 3\%$, assuming that 1/3 of all massive stars in the Galaxy may produce HeS stars, if they overflow their Roche lobes before completion of stable core He burning. This number may be an overestimate. For stars more massive than $15 M_{\odot}$, the formation of HeS stars is possible in case B provided that they exhausted no more than 10–20% of the core He. The critical initial binary mass ratio, q_0 , that still allows a stable mass exchange hardly exceeds ~ 0.4 . Additionally, for the avoidance of runaway mass-loss and the formation of common envelopes with the further merger of companions, the progenitor binaries of HeS stars should not have initial orbital periods exceeding several hundred days.

We note that hot He-stars may have not only massive, but also intermediate-mass companions (see Fig. 7). For example, out of a system with a minimum HeS star progenitor’s mass of $7 M_{\odot}$ and $q_0 \geq 0.6$, a binary with $(1 + 4) M_{\odot}$ can be formed, and a $4 M_{\odot}$ star would appear as an early A-star.

In our analysis, we have discarded low-mass helium remnants cooler than $T_{\text{eff}} \approx 20\,000 \text{ K}$, but we plan to discuss this problem in the future.

Short-period binaries subject to case A mass exchange, with initial orbital periods, $P_0 = (2\text{--}5) \text{ days}$, may also give rise to HeS stars. Since IMF and distribution over P_0 favor their formation, they contribute about 30% of all HeS stars. Formation of HeS stars in case A is possible since in this case precursors of HeS stars are rapid rotators and rotation-induced effects reduce radius expansion of the main-sequence stars in very close binaries compared to more slowly rotating components in wider binaries (Heger & Langer 2000). The rotation effects allow some binary components to avoid the potential contact and possible coalescence on the main sequence.

We note that hot helium stars with masses $(1\text{--}10) M_{\odot}$ are supposed to experience short-period radial pulsations accompanied by the formation of periodic shock waves (Fadeyev & Novikova 2003). More massive WR stars experience radial and non-radial pulsations as well (e.g., Nazé et al. 2021). We plan to investigate pulsations of the intermediate-mass evolved helium stars in a separate paper (Fadeyev et al., in prep.).

Selection effects reduce the number of potentially observable Galactic HeS stars. In the visual range, a hot He star emitting mostly in UV is extremely difficult to discover in a binary, because its companion is a cooler and brighter B or Be-star (Fig. 7). This effect will reduce the number of observable HeS stars by at least a factor of two (Fig. 7). More detailed spectral model calculations are required to improve these estimates using the atmospheric parameters and chemical composition of the synthesized HeS population (Fig. 10).

In our study, we have assumed that stellar winds of HeS stars obey the empirical Nugis & Lamers (2000) law. However, the issue of stellar winds from hot helium stars is not solved as of yet. Vink (2017) suggested a model of radiation-driven mass-loss wind for He stars that predicts mass-loss rates by an order

of magnitude lower than Nugis & Lamers’ law. Götberg et al. (2023) claim that some of the stripped stars discovered in the SMC obey Vink’s law, while some of them possess even weaker winds. As the problem remains unsolved, we performed several test calculations comparing the influence of Nugis-Lamers’ and Vink’s winds upon the masses of retained H/He envelopes and their chemical composition. Plots with results are presented in Appendices A and B. As could be expected, Nugis-Lamers winds result in lower masses of envelopes at the He-burning part of the evolutionary tracks and lower He abundances. However, the difference in the envelope masses for considered models is only (5–7)%.

We conclude that, according to present binary evolution models, there are expected to be a few thousand HeS stars in massive binary systems in the Galaxy. Still, this population of hot He-rich stars remains hidden. Future work to better understand the selection effects and predict the observational signatures of HeS stars in binaries is needed to tailor observing campaigns aimed at discovering these elusive products of binary evolution.

Acknowledgements. The authors thank the anonymous referee for useful notes and suggestions. The authors acknowledge fruitful discussions with Dr. N. Chugai. L. Yungelson acknowledges support via the German Academic Exchange Service DAAD Research Stays for University Academics and Scientists Program. A. Kuranov acknowledges support by the Russian Science Foundation grant 21-12-00141 (calculations of evolutionary models using the MESA code). This research has made use of the NASA’s Astrophysics Data System Bibliographic Services and of the SIMBAD database, operated at CDS, Strasbourg, France.

References

- Barbaro, G., Giannone, P., Giannuzzi, M. A., & Summa, C. 1969, in Mass Loss from Stars, ed. M. Hack, *Astrophys. Space Sci. Lib.*, 13, 217
- Barría, D., Mennickent, R. E., Schmidtobreick, L., et al. 2013, *A&A*, 552, A63
- Bodensteiner, J., Shenar, T., Mahy, L., et al. 2020, *A&A*, 641, A43
- Chanlaridis, S., Antoniadis, J., Aguilera-Dena, D. R., et al. 2022, *A&A*, 668, A106
- Chomiuk, L., & Povich, M. S. 2011, *AJ*, 142, 197
- Crowther, P. A. 2015, in *Wolf-Rayet Stars*, eds. W. R. Hamann, A. Sander, & H. Todt, 21
- de Jager, C., Nieuwenhuijzen, H., & van der Hucht, K. A. 1988, *A&AS*, 72, 259
- de Kool, M. 1990, *ApJ*, 358, 189
- De Loore, C., de Grève, J. P., van den Heuvel, E. P. J., & de Cuyper, J. P. 1974, *Mem. Soc. Astron. It.*, 45, 893
- de Mink, S. E., Langer, N., & Izzard, R. G. 2011, in *Active OB Stars: Structure, Evolution, Mass Loss, and Critical Limits*, eds. C. Neiner, G. Wade, G. Meynet, & G. Peters, 272, 531
- Dessart, L., Yoon, S.-C., Aguilera-Dena, D. R., & Langer, N. 2020, *A&A*, 642, A106
- Dionne, D., & Robert, C. 2006, *ApJ*, 641, 252
- Doughty, C., & Finlator, K. 2021, *MNRAS*, 505, 2207
- Drout, M. R., Götberg, Y., Ludwig, B. A., et al. 2023, arXiv e-prints [arXiv:2307.00061]
- Ekström, S., Georgy, C., Eggenberger, P., et al. 2012, *A&A*, 537, A146
- El-Badry, K., & Burdge, K. B. 2022, *MNRAS*, 511, 24
- El-Badry, K., Conroy, C., Quataert, E., et al. 2022, *MNRAS*, 516, 3602
- Fadeyev, Y. A., & Novikova, M. F. 2003, *Astron. Lett.*, 29, 522
- Gagnier, D., & Pejcha, O. 2023, *A&A*, 674, A121
- Geier, S. 2020, *A&A*, 635, A193
- Giannone, P., & Giannuzzi, M. A. 1972, *A&A*, 19, 298
- Giannone, P., Refsdal, S., & Weigert, A. 1970, *A&A*, 4, 428
- Gies, D. R., Wang, L., & Klement, R. 2023, *ApJ*, 942, L6
- Götberg, Y., de Mink, S. E., & Groh, J. H. 2017, *A&A*, 608, A11
- Götberg, Y., de Mink, S. E., Groh, J. H., et al. 2018, *A&A*, 615, A78
- Götberg, Y., Drout, M. R., Ji, A. P., et al. 2023, *ApJ*, 959, 125
- Habets, G. M. H. J. 1986, *A&A*, 167, 61
- Hainich, R., Ramachandran, V., Shenar, T., et al. 2019, *A&A*, 621, A85
- Hamann, W. R., Gräfener, G., Liermann, A., et al. 2019, *A&A*, 625, A57
- Han, Z., Podsiadlowski, P., Maxted, P. F. L., Marsh, T. R., & Ivanova, N. 2002, *MNRAS*, 336, 449

- Han, Z., Podsiadlowski, P., Maxted, P. F. L., & Marsh, T. R. 2003, [MNRAS](#), **341**, 669
- Harmanec, P. 1970, [Ap&SS](#), **6**, 497
- Heber, U. 2016, [PASP](#), **128**, 082001
- Heger, A., & Langer, N. 2000, [ApJ](#), **544**, 1016
- Heger, A., Langer, N., & Woosley, S. E. 2000, [ApJ](#), **528**, 368
- Hennicker, L., Kee, N. D., Shenar, T., et al. 2022, [A&A](#), **660**, A17
- Howarth, I. D., & Heber, U. 1990, [PASP](#), **102**, 912
- Iben, I., Jr., & Tutukov, A. V. 1985, [ApJS](#), **58**, 661
- Iben, I., Jr., & Tutukov, A. V. 1987, [ApJ](#), **313**, 727
- Irrgang, A., Przybilla, N., & Meynet, G. 2022, [Nat. Astron.](#), **6**, 1414
- Ivanova, N., Justham, S., Chen, X., et al. 2013, [A&ARv](#), **21**, 59
- Kanarek, G. C. 2017, PhD Thesis, Columbia University, New York, USA
- Kim, H.-J., Yoon, S.-C., & Koo, B.-C. 2015, [ApJ](#), **809**, 131
- Kippenhahn, R. 1969, [A&A](#), **3**, 83
- Kippenhahn, R., & Meyer-Hofmeister, E. 1977, [A&A](#), **54**, 539
- Kippenhahn, R., & Weigert, A. 1967, [Z. Astrophys.](#), **65**, 251
- Kippenhahn, R., Kohl, K., & Weigert, A. 1967, [Z. Astrophys.](#), **66**, 58
- Klement, R., Baade, D., Rivinius, T., et al. 2022, [ApJ](#), **940**, 86
- Klencki, J., Istrate, A., Nelemans, G., & Pols, O. 2022, [A&A](#), **662**, A56
- Kriz, S., & Harmanec, P. 1975, [Bull. Astron. Inst. Czechoslov.](#), **26**, 65
- Langer, N., Wellstein, S., & Petrovic, J. 2003, in [A Massive Star Odyssey: From Main Sequence to Supernova](#), eds. K. van der Hucht, A. Herrero, & C. Esteban, 212, 275
- Lauterborn, D. 1970, [A&A](#), **7**, 150
- Licquia, T. C., & Newman, J. A. 2015, [ApJ](#), **806**, 96
- Liu, J., Zhang, H., Howard, A. W., et al. 2019, [Nature](#), **575**, 618
- Menon, A., Langer, N., de Mink, S. E., et al. 2021, [MNRAS](#), **507**, 5013
- Nazé, Y., Rauw, G., & Gosset, E. 2021, [MNRAS](#), **502**, 5038
- Nomoto, K., Yamaoka, H., Pols, O. R., et al. 1994, [Nature](#), **371**, 227
- Nugis, T., & Lamers, H. J. G. L. M. 2000, [A&A](#), **360**, 227
- Ohlmann, S. T., Röpke, F. K., Pakmor, R., & Springel, V. 2016, [ApJ](#), **816**, L9
- Öpik, E. 1924, [Publications of the Tartu Astrofizika Observatory](#), **25**, 1
- Packet, W. 1981, [A&A](#), **102**, 17
- Paczyński, B. 1967, [Acta Astron.](#), **17**, 355
- Paxton, B., Bildsten, L., Dotter, A., et al. 2011, [ApJS](#), **192**, 3
- Paxton, B., Cantefio, M., Arras, P., et al. 2013, [ApJS](#), **208**, 4
- Paxton, B., Marchant, P., Schwab, J., et al. 2015, [ApJS](#), **220**, 15
- Paxton, B., Schwab, J., Bauer, E. B., et al. 2018, [ApJS](#), **234**, 34
- Paxton, B., Smolec, R., Schwab, J., et al. 2019, [ApJS](#), **243**, 10
- Pecaut, M. J., & Mamajek, E. E. 2013, [ApJS](#), **208**, 9
- Petrovic, J., Langer, N., & van der Hucht, K. A. 2005, [A&A](#), **435**, 1013
- Podsiadlowski, P. 1996, in [Hydrogen Deficient Stars](#), eds. C. S. Jeffery, & U. Heber, [ASP Conf. Ser.](#), **96**, 419
- Pols, O. R., Cote, J., Waters, L. B. F. M., & Heise, J. 1991, [A&A](#), **241**, 419
- Popova, E. I., Tutukov, A. V., & Yungelson, L. R. 1982, [Ap&SS](#), **88**, 55
- Ramachandran, V., Klencki, J., Sander, A. A. C., et al. 2023, [A&A](#), **674**, L12
- Refsdal, S., & Weigert, A. 1969, in [Mass Loss from Stars](#), ed. M. Hack, [Astrophys. Space Sci. Lib.](#), **13**, 253
- Rosales Guzmán, J. A., Mennickent, R. E., Djurašević, G., Araya, I., & Curé, M. 2018, [MNRAS](#), **476**, 3039
- Sander, A. A. C., Hamann, W. R., Todt, H., et al. 2019, [A&A](#), **621**, A92
- Schaffenroth, V., Pelisoli, I., Barlow, B. N., Geier, S., & Kupfer, T. 2022, [A&A](#), **666**, A182
- Sen, K., Langer, N., Marchant, P., et al. 2022, [A&A](#), **659**, A98
- Shenar, T., Bodensteiner, J., Abdul-Masih, M., et al. 2020a, [A&A](#), **639**, L6
- Shenar, T., Gilkis, A., Vink, J. S., Sana, H., & Sander, A. A. C. 2020b, [A&A](#), **634**, A79
- Shenar, T., Wade, G. A., Marchant, P., et al. 2023, [Science](#), **381**, 761
- Sravan, N., Marchant, P., Kalogera, V., Milisavljevic, D., & Margutti, R. 2020, [ApJ](#), **903**, 70
- Tsujimoto, M., Hayashi, T., Morihana, K., & Moritani, Y. 2023, [PASJ](#), **75**, 177
- Tutukov, A., & Yungelson, L. 1987, in [IAU Colloq. 95: Second Conference on Faint Blue Stars](#), eds. A. G. D. Philip, D. S. Hayes, & J. W. Liebert, 435
- Tutukov, A. V., & Yungelson, L. R. 1990, [Sov. Astron.](#), **34**, 57
- Tutukov, A., Yungelson, L., & Klayman, A. 1973, [Nauchnye Informatsii](#), **27**, 3
- Uomoto, A. 1986, [ApJ](#), **310**, L35
- Villaseñor, J. I., Lennon, D. J., Picco, A., et al. 2023, [MNRAS](#), **525**, 5121
- Vink, J. S. 2017, [A&A](#), **607**, L8
- Vink, J. S., de Koter, A., & Lamers, H. J. G. L. M. 2001, [A&A](#), **369**, 574
- Waldman, R., Yungelson, L. R., & Barkat, Z. 2008, in [Hydrogen-Deficient Stars](#), eds. A. Werner, & T. Rauch, [ASP Conf. Ser.](#), **391**, 359
- Wang, L., Gies, D. R., Peters, G. J., & Han, Z. 2023, [AJ](#), **165**, 203
- Webbink, R. F. 1984, [ApJ](#), **277**, 355
- Yoon, S. C., Woosley, S. E., & Langer, N. 2010, [ApJ](#), **725**, 940
- Yoon, S.-C., Dessart, L., & Clocchiatti, A. 2017, [ApJ](#), **840**, 10
- Yungelson, L. R., & Tutukov, A. V. 2005, [Astron. Rep.](#), **49**, 871
- Zak, J., Jones, D., Boffin, H. M. J., et al. 2023, [MNRAS](#), **524**, 5749
- Ziółkowski, J. 1970, [Acta Astron.](#), **20**, 213

Appendix A: Dependence of evolutionary tracks and masses of envelopes of hot helium stars on accepted stellar wind law

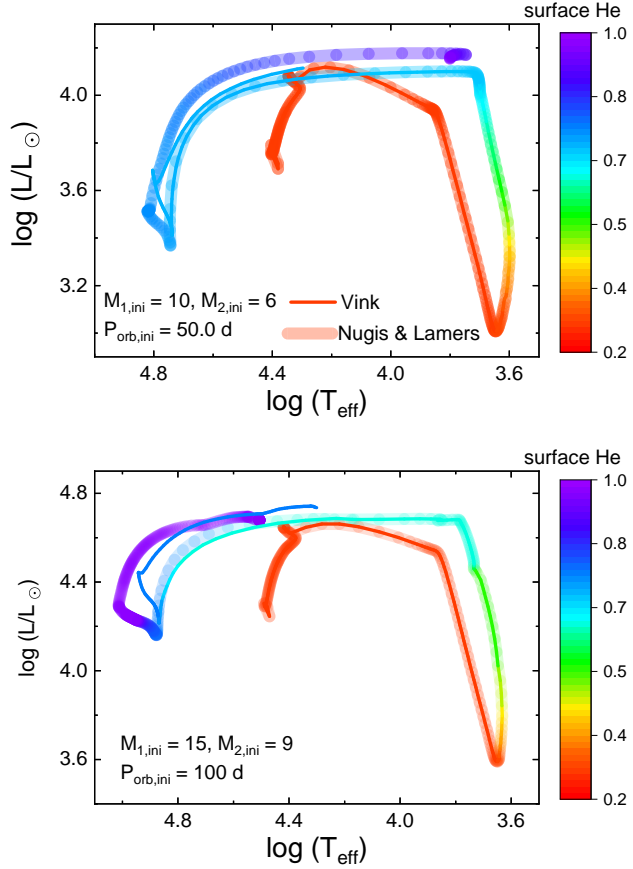


Fig. A.1. HRD for the primary component of a $10+6 M_{\odot}$ binary with $P_0 = 50$ days (*upper panel*) and a $15+9 M_{\odot}$ binary with $P_0 = 100$ days (*lower panel*) forming HeS stars for wind mass-loss laws of HeS stars according to [Nugis & Lamers \(2000\)](#) and [Vink \(2017\)](#) (the thin and thick lines, respectively.) The color scale to the right codes the surface He abundance Y .

Appendix B: Dependence of the surface chemical composition of a hot helium star on the stellar wind law

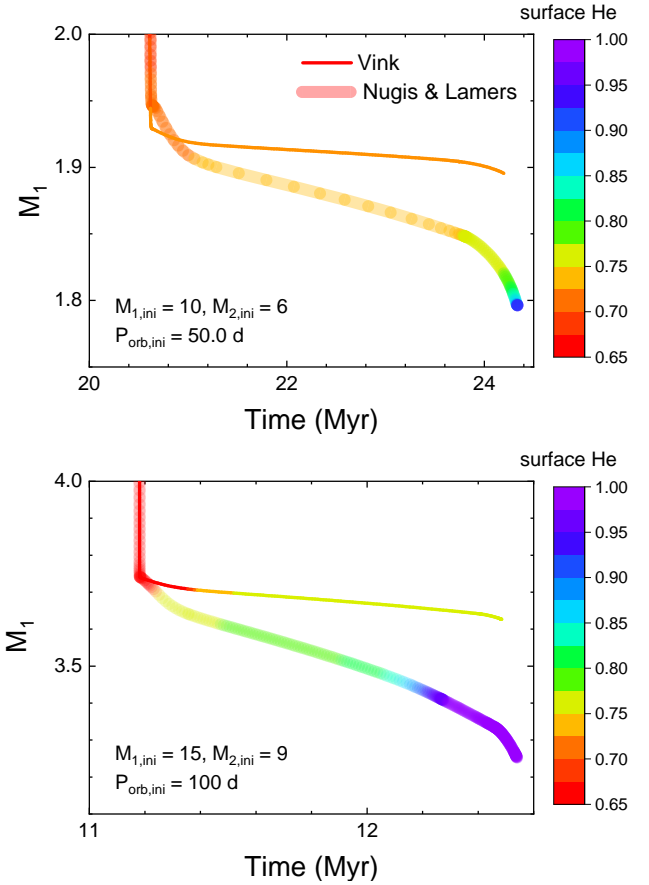


Fig. B.1. Time dependence of the HeS mass formed from binaries shown in Fig. A.1 for different HeS star stellar wind mass-loss laws. The color scale to the right codes the surface He abundance Y .